communications engineering

Article

https://doi.org/10.1038/s44172-024-00317-x

Synergetic pyrolysis of lithium-ion battery cathodes with polyethylene terephthalate for efficient metal recovery and battery regeneration

Check for updates

Zhe Meng[1,2,5], Jinchuan Dai[1,5], Xiao-Ying Lu[3], Kehua Wu[3], Yonghong Deng[4], Jun Wang[4], Kaimin Shih[2] & Yuanyuan Tang[1]

Spent $LiNi_xCo_yMn_zO_2$ ($x+y+z=1$) and polyethylene terephthalate are major solid wastes due to the growing Li-ion battery market and widespread plastic usage. Here we propose a synergistic pyrolysis strategy to recover valuable metals by thermally treating $LiNi_{1/3}Co_{1/3}Mn_{1/3}O_2$ and polyethylene terephthalate. With polyethylene terephthalate assistance, $LiNi_{1/3}Co_{1/3}Mn_{1/3}O_2$ decomposes at 400 °C, and fully converts to Li_2CO_3, MnO, and Ni-Co alloy at 550 °C within 30 min, using a 1.0:0.3 mass ratio of $LiNi_{1/3}Co_{1/3}Mn_{1/3}O_2$ to polyethylene terephthalate. Furthermore, density functional theory calculations confirm the preference for O-Li bonding. Surface adsorption and free radical/gaseous reduction reactions explain the role of polyethylene terephthalate in promoting lattice destruction. The complete decomposition facilitates efficient post-treatment, achieving over 99% recovery of Li, Ni, Co, and Mn via water washing. Regenerated $LiNi_{1/3}Co_{1/3}Mn_{1/3}O_2$ was synthesized by using recovered Li- and transition metal-containing products as feedstocks. This study provided a chemical-free, energy-saving, and scalable recovery strategy while addressing polyethylene terephthalate waste minimization.

To meet the global requirement of energy supply and reduction in greenhouse gas emission, the market of electric vehicles has been developing and increasing rapidly over the years and is anticipated to exceed 300 million in 2030[1,2]. The lithium-ion batteries (LIBs), especially with the $LiNi_xCo_yMn_zO_2$ ($x+y+z=1$, NCM) cathode materials, have been intensively investigated for electrochemical energy storage, owing to high energy density, high cell voltage, and high reliability, etc., thus serving as the leading battery packs for electric vehicle applications[3–5]. It is predicted that the global market for NCM cathode materials could reach US 46.4$ billion by 2027[6]. However, the exploding market of LIBs is translating into tremendous number of discarded ones, due to the limited service life time[2]. In addition to the challenge of waste storage, spent LIBs contain hazardous materials like heavy metals (e.g., Ni and Co) and toxic electrolytes which are extremely harmful to both environment and human health. In the meantime, the metal elements in cathode materials, including Li, Ni, Co, and Mn, are of high value while facing severe problems of resource depletion[7]. Thus, it is of implication for both environment and economy to search for an environmentally friendly metal recycling strategy from NCM cathode materials in spent LIBs.

With the advantages of large treatment capacity and simple operation procedures, pyrometallurgical treatments have already gained considerable attention with continuous research efforts in the field of metal recovery from the spent LIBs. Aided by chemical reactions under elevated temperatures, pyrometallurgy treatment can destruct the lithiated metal oxides and separate them into metal fractions that can be reclaimed via simple post treatments. Traditional pyrometallurgy, which has been widely adopted in many countries, always transforms the waste battery strips into metal alloys at high temperatures[3,8–10]. However, the high energy consumption hinders economic interests, and the inevitable loss of lithium during pyrolysis process remains a technical hurdle as well. To reduce treatment cost and enhance metal recovery, extensive studies have been conducted with participation of chemicals during thermal treatments, including gas, salt, and other reducing agents. Chlorination or sulfation salts and mineral acids have

[1]Guangdong Provincial Key Laboratory of Soil and Groundwater Pollution Control, School of Environmental Science and Engineering, Southern University of Science and Technology, Shenzhen, China. [2]Department of Civil Engineering, The University of Hong Kong, Hong Kong SAR, China. [3]Faculty of Science and Technology, Technological and Higher Education Institute of Hong Kong, Hong Kong SAR, China. [4]Department of Materials Science and Engineering, Southern University of Science and Technology, Shenzhen, China. [5]These authors contributed equally: Zhe Meng, Jinchuan Dai. e-mail: tangyy@sustech.edu.cn

been added to the roasting process and could convert Li into soluble LiCl or Li_2SO_4[11–14]. For example, NCM was successfully decomposed into Li and transition metal (TM) salts after 750 °C-calcination with 100 wt% Na_2SO_4 addition[15]. Although the reaction temperature can be reduced by studies above via transferring reaction pathways, the consumption of salts or acids is high and even up to twice that of spent cathode materials in mass, causing subsequent problems of waste salts and gaseous exhausts. Therefore, some other studies have paid attention to carbon-containing reductants as the cleanest reducing agents, e.g., lignite, graphite, etc.[16,17]. LCO/NCM can be decomposed and reduced to a low valence stage (Li_2CO_3, transition metal elements, and oxides) without the use of inorganic acid during the thermal treatment. For example[18], previous work reported the destruction and collapse of oxygen octahedrons of NCM at around 750 °C, and the reaction processes were controllable by governing the amount of additives. However, the recovery ratio of each metal elements varied a lot from 81% to 100%, implying that a further decrease in reaction temperatures was expected to enhance its economic feasibility[1,3,19,20]. Thus, it still remains an urgent need and key issue to develop a chemical-free recycling strategy that is more energy-saving and efficient.

As one of the most consumed polymer resins, polyethylene terephthalate (PET) is widely applied in various fields like packaging, drinking bottles, and construction industries, thus contributing to a tremendous volume of PET production and waste generation. The most current statistics reported that the global market volume of PET reached nearly 23.7 million metric tons in 2020 and was expected to grow to 29.7 million metric tons by 2026. However, the majority of PET ended up as solid wastes[21], causing serious environmental concerns to the ocean, soil, organisms, and human beings. The pyrolysis of plastic wastes, including PET, has been widely studied, as it can effectively utilize the plastic wastes as fuel sources and reduce the waste volume at the same time. During PET pyrolysis, the oxygenated functional groups break and escape from the polymer chain. As a result, the PET was quickly decomposed at over 400 °C, generating large amounts of free radicals and gases for secondary reactions[22–24]. Previous studies have reported that the PET-HDPE co-pyrolyzation reduced the pyrolysis temperature of HDPE while delayed PET decomposition and altered the product compositions, and all plastic pyrolysis was delayed when PET was mixed with PP and PS due to the volatile products[24,25]. These studies revealed that plastic was likely to affect the pyrolysis behavior of other components by releasing pyrolysis products. Based on the aforementioned pyrolysis properties and performance of the PET, a battery material recovery strategy can be expected by addition of PET plastics to the pyrolysis reactions of the NCM cathode materials. It is hypothesized that PET and its intermediate pyrolysis products could react with and deconstruct the crystal lattice of NCM materials, therefore converting target metals into separated and easy-collected phases. The proposed strategy might provide a technical solution for resource utilization of spent NCM and waste PET plastics at the same time, and simultaneously reduce energy consumption because of the synergy effects. Only C, H, and O are introduced into the reaction system, without the use and production of inorganic chemicals, which can make the reaction process environmentally friendly.

Besides reaction feasibility, the reaction mechanisms should be intensively explicated to provide theoretical basis for scale-up and migration application in metal recovery industries. In recent years, density functional theory (DFT) has become the most popular theoretical framework for studying surface electron structure of battery materials[26]. By means of DFT, the (001) surface of layered $LiCoO_2$ (LCO) was reported to have relative lower surface energy, compared with other surfaces of LCO. Thus, (001) surface was proven stable in LCO crystal strucutre[27,28]. Previous work optimized the adsorption structure of LCO and sulfur species, proving that the LCO-S(IV) anchor played a vital role in the reaction progresses. Therefore, it can be anticipated that the DFT calculation can aid in optimizing the adsorption configuration and adsorption energy between PET and NCM, which may further provide the combination preference at atomic level. In addition, the mass spectra (MS) and Fourier transform infrared spectrometer (FT-IR) coupled with thermal gravimetric analyzer (TGA) have been widely used in plastic pyrolysis studies[29] which revealed the synergy effect by monitoring the pyrolysis behaviors via TGA-MS-FTIR and comparing the blended systems with the pure materials.

To sum up, in order to solve the problem of NCM recycle, researchers have carried out many studies about using pyrometallurgy strategies which are regarded as more feasible in up-scale application. Despite progress in applying effective reductants like carbon, current strategies still face challenges like high energy consumption, high chemical usage, or low recovery efficiency. Therefore, it is highly desirable to develop energy-saving process for pyrolysis recycling of battery materials to achieve economic and environmental feasibility. It is well known that PET is one of the most widely used polymers for disposable plastic products, which contributed to a tremendous volume of waste generation. PET can be decomposed into fuel sources by catalytic reactions, with simultaneous generation of large amounts of free radicals and gases, which could greatly reduce the pyrolysis temperature for the thermal decomposition of the other co-pyrolyzation substances. However, its behavior when pyrolized together with metals is still lack of study. Therefore, this study proposed a NCM-PET synergetic pyrolysis strategy to recycle valuable metals in NCM cathode materials, with the addition of PET plastics as chemical additives. The effect of pyrolysis parameters on reaction processes was comprehensively explored and the pyrolysis conditions were optimized as well. The recovery process was developed, including water washing after synergetic pyrolysis, filtration, and evaporation, which was totally chemical free. After metal recovery, new NCM materials were regenerated by employing the recovery products as reaction feedstocks. Finally, we proposed the theory of synergy pyrolysis behavior of NCM-PET system and deeply discussed its mechanisms by integrating both experimental characterization and DFT theoretical calculation. The mechanism study provided theoretical verification and guidance for future scale-up and migration applications. The proposed strategy in this study aimed at providing a "waste-to-resource" solution for both PET and NCM wastes that possessed superior economic and environmental benefits.

Results

Decomposition behavior of NCM via synergetic pyrolysis

As shown in Fig. 1a, the pyrolysis behavior of NCM could be regarded as a stepwise reduction and decomposition along with the elevated temperatures. Peaks of NCM, as the primary crystal phase, were found declining slightly after 400 °C pyrolysis. Meanwhile, three lithium manganese oxides ($Li_{0.5}MnO_2$, Li_3MnO_4, $LiMnO_4$) were observed with tiny peaks, which were attributed to the reconstruction of Li and TM atoms under the pyrolysis condition. The partial destruction of the NCM crystals could lead to the formation of new crystal phases. When the temperature was increased to 500 °C, the peaks of NCM cannot be observed and the three lithium manganese oxides still existed without obvious changes in peak intensity. Moreover, the peaks of Li_2CO_3, $NiMnO_3$, $Ni_xCo_{1-x}O$, and Ni_xCo_{1-x} were identified, indicating that some of the Ni and Co were partially reduced from trivalent to divalent ($Ni_xCo_{1-x}O$) and zero valent (Ni_xCo_{1-x}). When the temperature was further elevated to 550 °C, three lithium manganese oxides and $NiMnO_3$ were eliminated and replaced with Li_2CO_3 peaks. When the pyrolysis temperature reached 600 °C, NCM was fully decomposed to Li_2CO_3, MnO and Ni_xCo_{1-x}, while the peaks of $Ni_xCo_{1-x}O$ were not detectable. The types of crystal phases remained unchanged with further treatment from 700 to 800 °C, but peak intensities due to increasing crystallization of Li_2CO_3, MnO and Ni_xCo_{1-x} were clearly observed. When the temperature reached 900 °C, Li_2CO_3 suddenly disappeared while LiC was observed with low peak intensity. This was possibly due to the decomposition and carbonization of Li_2CO_3. In addition, the peaks of MnO and Ni_xCo_{1-x} remained unchanged, when compared with the XRD patterns of samples pyrolyzed at 800 °C. When the sample was pyrolyzed at 1000 °C, it is interesting that LiC, Mn_xNi_{1-x}, and Mn_xCo_{1-x} were found in the XRD patterns, thus illustrating that the TM (Ni, Co, and Mn) were finally reduced to zero valence with the formation of solid solutions. The phase transformation of Ni, Co, and Mn represented a gradual reduction of Mn(IV), Ni(II), and Co(III) to Mn (0), Ni (0), and Co (0), respectively.

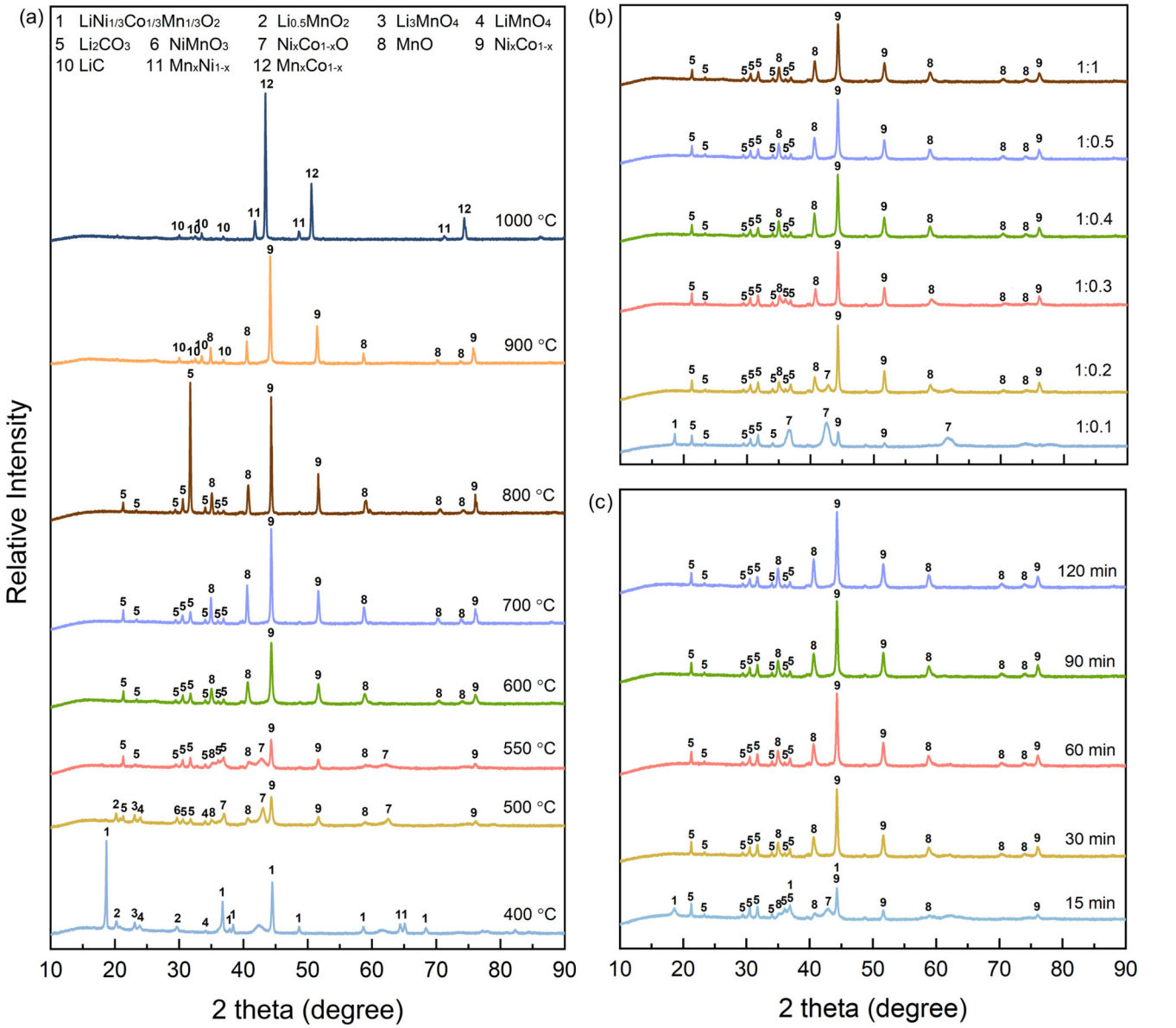

Fig. 1 | Typical X-ray diffraction (XRD) patterns of the PET+NCM ($LiNi_{1/3}Co_{1/3}Mn_{1/3}O_2$) synergetic pyrolysis products. a XRD patterns of the products obtained at different temperatures (400, 500, 550, 600, 700, 800, 900 and 1000 °C) for 120 min, with a mass ratio of NCM/PET of 1.0:1.0, (**b**) XRD patterns of the products with various mass ratios of NCM/PET (1.0:0.1; 1.0:0.2, 1.0:0.3, 1.0:0.4, 1.0:0.5 and 1.0:1.0) at 600 °C for 120 min, and (**c**) XRD patterns of the pyrolized products of different time (15, 30, 60, 90 and 120 min) at 600 °C, with a mass ratio of NCM/PET of 1.0:0.3. PET stands for polyethylene terephthalate.

Furthermore, Fig. 1b revealed the effect of NCM/PET mass ratio on the reaction series under 600 °C pyrolysis. When a small amount of PET was mixed with NCM (NCM:PET mass ratio of 1.0:0.1), NCM was not fully decomposed with a remaining peak at 18.7°. Meanwhile, Li_2CO_3, $Ni_xCo_{1-x}O$, and Ni_xCo_{1-x} were observed as the product phases, due to the thermal decomposition of NCM. When the NCM:PET ratio was changed to 1.0:0.2, the crystal phase of NCM was completely diminished with the peaks of Ni_xCo_{1-x} and MnO growing but $Ni_xCo_{1-x}O$ decreasing. When the NCM:PET ratio was varied to 1.0:0.3, the disappearance of $Ni_{1-x}Co_{1-x}O$ was found, probably due to its reduction to zero-valent metals. Interestingly, extra PET addition (NCM:PET = 1.0:1.0) showed no influence on the phase composition and peak intensity of the products. To investigate the effect of PET addition on crystal phase change in the reaction system, pure NCM was also pyrolyzed under nitrogen atmosphere and the corresponding XRD pattern was given in Supplementary Fig. S1. It is revealed that no crystal phase transformation occurred for the pure NCM sample, even elevated to 600 °C. Therefore, the comparison implied that PET played a pivotal role in the decomposition of NCM sample. PET (or its pyrolysis products) could stimulate the structure collapse of NCM for efficient separation of Li and TM, and simultaneously possess reducibility to transform Ni/Co(II) into alloys. The effect of pyrolysis duration time on crystal phase change was further presented in Fig. 1c. It is obvious that the majority of NCM was quickly decomposed into Li_2CO_3, $Ni_xCo_{1-x}O$, Ni_xCo_{1-x}, and MnO within only 15 min. After 30 min, the peaks of NCM fully disappeared and the $Ni_xCo_{1-x}O$ phase also vanished, and meanwhile, the peaks of Ni_xCo_{1-x} were heightened, owing to continuous reduction of Ni and Co. With the increase of pyrolysis time from 60 min to 120 min, no obvious change in XRD patterns for the pyrolyzed products, thus implying that the phase transformation terminated within 30 min. To demonstrate the effectiveness of NCM-PET synergetic pyrolysis strategy, the metal recovery ratio was calculated for the pyrolyzed products under different temperatures (Fig. 2). The element Li, Ni, Co, and Mn were about 100% remained in the solid phase products, given that the pyrolysis temperature was no higher than 700 °C. With the further increase of pyrolysis temperatures, the Li was lost

by 4% at 800 °C, while the recovery ratio of Ni, Co, and Mn was dropped by 5–7% at 900 °C. Therefore, to minimize energy and chemical consumption and simplify product speciation, the optimal parameters for the synergetic pyrolysis were set as 550 °C, 30 min and NCM:PET mass ratio of 1.0:0.3. The as-obtained product under the optimal conditions was denoted as Sample SP in the following studies. Furthermore, Fig. 3 demonstrated the element distribution of Sample SP by TEM elemental mapping, with the observation of both plate-like polygonal particles and granular ones (Fig. 3a). The polygonal particles, with a typical diameter of ~200 nm, were concentrated by Mn and O coincidently, which confirmed the formation of MnO as detected by XRD technique. The granular particles were much smaller in diameter (~100 nm), with only Ni and Co distributed uniformly, indicating the formation of Ni and Co solid solutions. As the distribution of Ni and Co is highly overlapped and Ni_xCo_{1-x} diffraction peaks were detected in XRD, the formation of Ni and Co solid solutions was thus concluded.

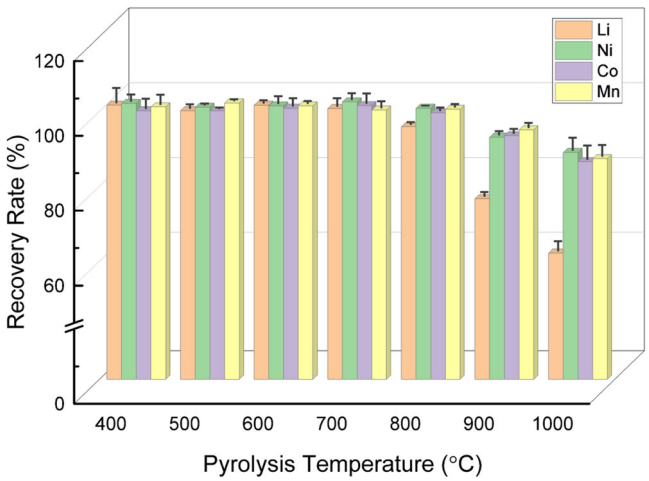

Fig. 2 | Recovery ratio of different metals (Li, Ni, Co, and Mn) in the pyrolyzed products obtained at various pyrolysis temperatures, and each data were provided with an error bar which was calculated via standard deviation of three parallel tests.

Degradation behavior of PET via synergetic pyrolysis

The mass losses with the elevated temperatures were analyzed to understand the thermal behavior of the blended NCM-PET system. As shown in Fig. 4a, the synergetic pyrolysis displayed a three-stage process, when pyrolysis temperature was gradually increased from room temperature to 1000 °C. To be specific, stage 1 took place between 310–549 °C, in which the mass dropped rapidly by 32.8% and the peak rate of mass loss occurred at 429 °C. Stage 2 was relatively prolonged and tardily with 14.0% of total mass lost from 549 to 643 °C, including two peaks of mass loss rate at 589 °C and 623 °C. Stage 3 could lead to a mass loss of 5.3% at 643–840 °C with a typical peak located at 713 °C. The mass change persisted at a very low rate after the temperature exceeding 840 °C. The start point of mass loss, which was mainly caused by PET degradation, was similar to the start point of NCM decomposition temperature, and showed a possibility of the synergetic pyrolysis effect. The volatile compounds released during pyrolysis were simultaneously monitored by combining FT-IR and MS measurements. The chemical structure of volatile products was revealed in the 3D FT-IR spectrum (Fig. 4b), and 2D FT-IR spectrum under representative temperatures (Fig. S6). To precisely identify the released gaseous species, the mass of each evolved species and its ion current was detected by the MS (Fig. 4c–m) measurement.

The peaks collected in 3D FT-IR spectrum indicated the release of various types of volatile compounds, including hydrocarbons (saturated, unsaturated and aromatic hydrocarbons), aldehydes, carboxyls, carbon oxides, and water. The formation of hydrocarbons was confirmed with the peak located at around 1380 cm^{-1} (the bending vibration of C-H bond) of the FT-IR spectra. The specific species were identified as CH_4, $C_2H\cdot$, $C_4H_3\cdot$, and $C_5H_5\cdot$ corresponding to the ion curves of $m/z = 15$, 25, 51, and 65 in

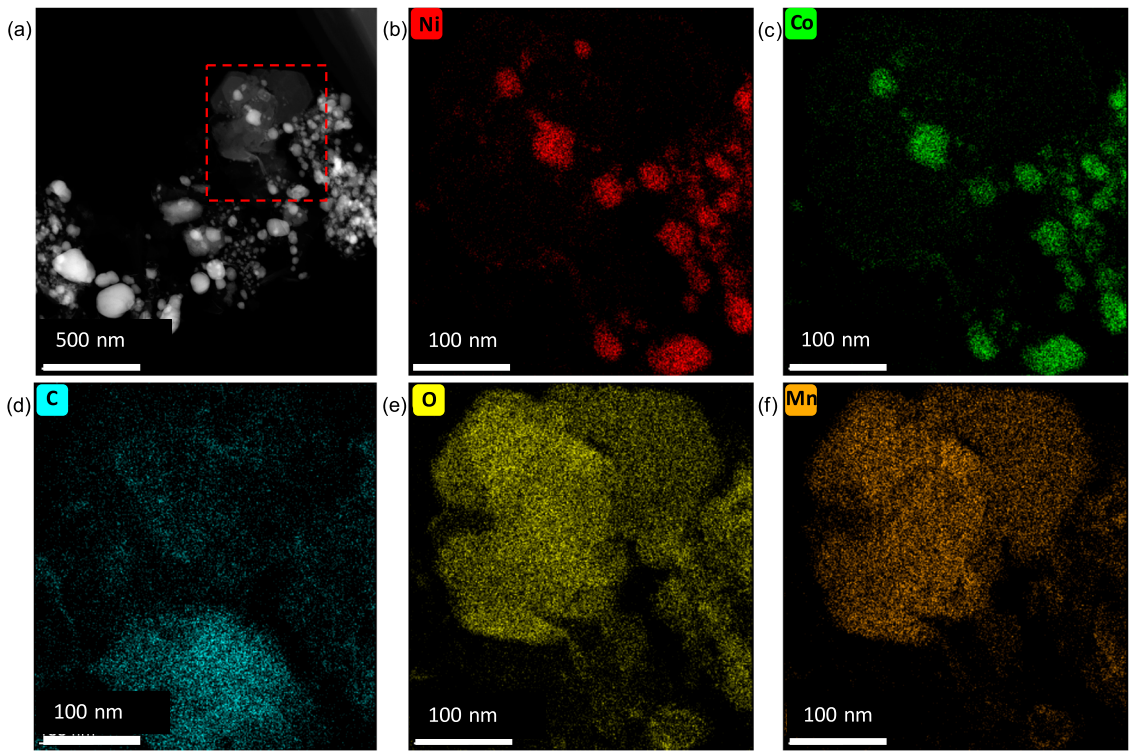

Fig. 3 | High-resolution TEM images of the pyrolyzed products (Sample SP) obtained under pyrolysis conditions of 550 °C, 30 min and a NCM ($LiNi_{1/3}Co_{1/3}Mn_{1/3}O_2$)/PET mass ratio of 1.0:0.3. a The TEM image of Sample SP, EDX mapping of elements including (**b**) Ni, (**c**) Co, (**d**) C, (**e**) O, and (**f**) Mn. PET stands for polyethylene terephthalate.

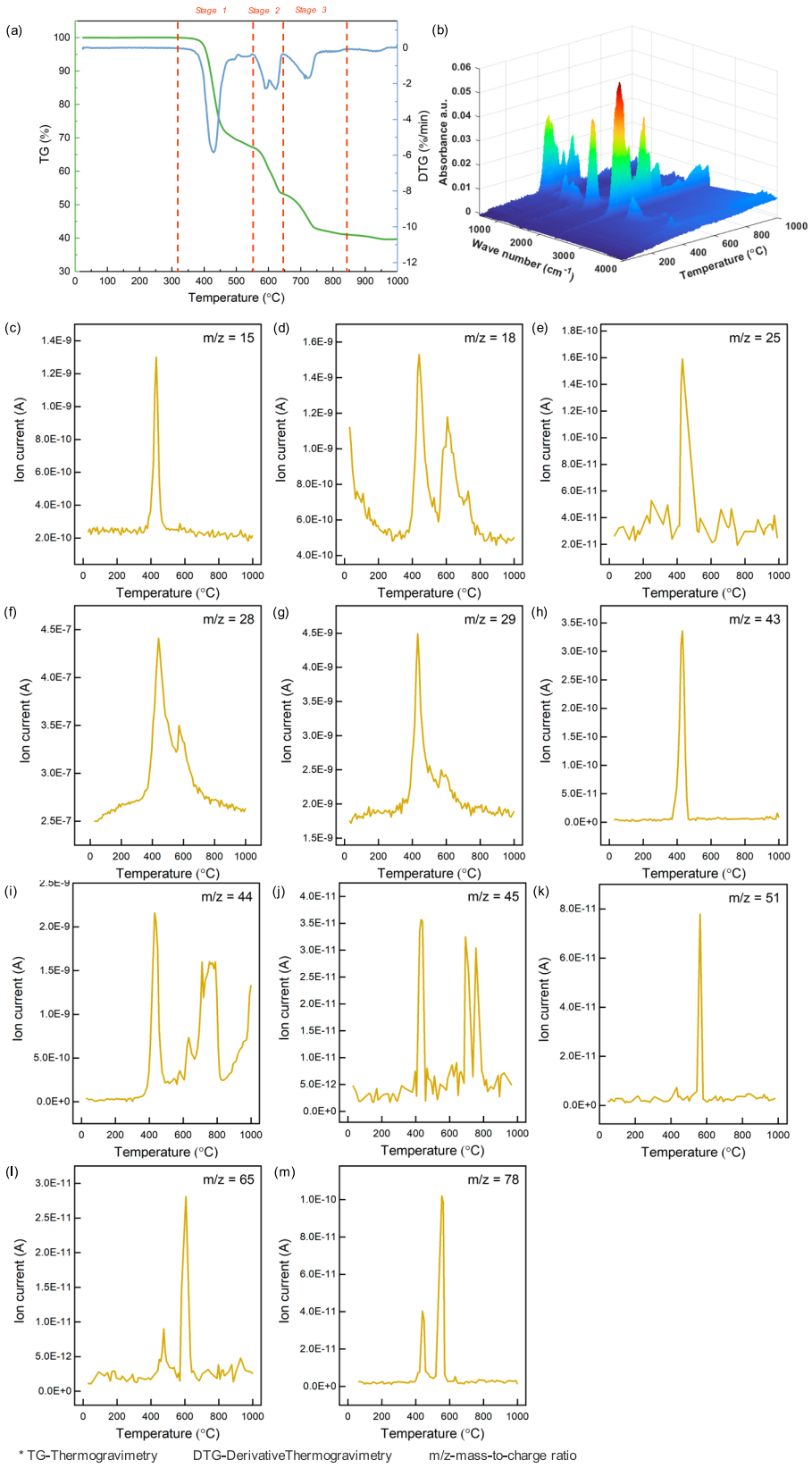

Fig. 4 | Thermogravimetric analysis and gaseous products during synergetic pyrolysis. a TG and DTG curves of PET + NCM ($LiNi_{1/3}Co_{1/3}Mn_{1/3}O_2$) mixture from 30 to 1000 °C, where PET is polyethylene terephthalate, and TG stands for thermogravimetry and DTG is derivative thermogravimetry; (**b**) 3-dimensional FT-IR spectra; and single ion curves in the gas released during TG analysis, including (**c**) m/z = 15, (**d**) m/z = 18, (**e**) m/z = 25, (**f**) m/z = 28, (**g**) m/z = 29, (**h**) m/z = 43, (**i**) m/z = 44, (**j**) m/z = 45, (**k**) m/z = 51, (**l**) m/z = 65 and (**m**) m/z = 78, where m/z is mass to charge ratio. The loaded mass ratio of NCM/PET was 1.0:1.0.

Fig. 4c, e, k, l, respectively. Among them, the CH_4 and C_2H· were released at Stage 1, while the C_4H_3· and C_5H_5· were mainly generated at Stage 2. Benzene was also observed as reflected in the single ion curve of $m/z = 78$ (Fig. 4m), and it was released at both Stage 1 and the early period of Stage 2 (before 600 °C). In addition to hydrocarbons, the formation of aldehyde groups was also suggested by the FT-IR results. The strong absorbance peak at around 1750 cm^{-1} was ascribed to the stretching vibration of C=O and the peak at 2820 cm^{-1} was attributed to the C-H stretching vibration in the aldehyde[24]. The ion curves of $m/z = 29$ (Fig. 4g) and 43 (Fig. 4h) were regarded as formyl radical and acetaldehyde, respectively. This indicated

Table 1 | Information for the optimized adsorption configurations of PET (polyethylene terephthalate) and NCM ($LiNi_{1/3}Co_{1/3}Mn_{1/3}O_2$) (001) slab

No.	Surface of NCM	Posture of PET	Bonding atoms	E_{ad} (eV)[a]
1	Li	horizontal	O-Li	−3.948
2	Li	horizontal	O-Li	−4.248
3	Li	horizontal	O-Li	−4.102
4	Li	vertical	O-Li	−1.080
5	Li	vertical	H-Li	−0.386
6	TM	horizontal	O-TM, C-TM	−2.757
7	TM	vertical	O-TM	−1.328
8	TM	vertical	O-TM	−0.843
9	TM	vertical	O-TM	−1.566
10	TM	vertical	H-TM	−0.832
11	O	horizontal	None	0.076

[a]E_{ads} is the calculated adsorption energy of specified adsorption configuration.

that the majority of these two aldehydes was evolved at Stage 1, while a small amount of formyl radicals was produced at Stage 2. Furthermore, the weak peaks at 3735–3580 cm^{-1} and 1084 cm^{-1} were correspondingly attributed to the vibration of O-H bond and stretching vibration of C-O bond, respectively, corresponding to the bending mode of ester and carboxylic acid. Thus, the $m/z = 45$ ion curve (Fig. 4j) could be identified as carboxyl acid radicals, according to the PET degradation behavior[22] throughout Stage 1, 2, and 3 until 800 °C. In addition, the intense peaks at 2439 cm^{-1} of the FT-IR spectra were the asymmetrical stretching vibration of C=O, which should be related to the formation of CO and CO_2 in ion curves with $m/z = 28$ (Fig. 4f) and 44 (Fig. 4i). Obviously, CO was mainly produced at Stage 1 and 2, while the CO_2 was gradually released at all three stages. Besides, the absorbance peaks at 1510 and 3739 cm^{-1} were coincident with the ion curve of $m/z = 18$, which represented that most of H_2O was also produced at the first two stages.

To summarize, PET plastics in the NCM blended system were mainly degraded at three reaction stages and the amount of the released gaseous products, including hydrocarbon (alkane, alkene, alkyne, and benzene), aldehyde, carboxylic acid, CO_2, CO, and H_2O, was gradually weakened from Stage 1 to Stage 3. According to previous studies[22,24,25,30,31], pure PET displayed a single but rapid degradation stage at 400–500 °C with a maximum degradation rate over 400 °C. The pyrolysis of pure PET began with the break of ester links, which caused chain scission and produced carboxylic acid and olefinic at the end of chains. Subsequently, the disintegration and secondary reactions continued till the end of degradation mainly by the repeated decarboxylation and free radical reactions. Thus, the decarboxylation and free radical reactions were the most pivotal and dominant mechanism for pure PET pyrolysis and were also considered as crucial step in synergetic pyrolysis of this study. As a comparison, the degradation of PET with NCM in this study was initiated at a similar temperature (400 °C), but the completion of degradation was delayed to Stage 3 at over 800 °C. Furthermore, similar gaseous species were detected in the PET-NCM system, when compared with the pure PET system. This indicated the similar degradation pathways in these two systems. For instance, the carboxylic acid was released throughout the three stages, indicating that the decarboxylation reaction was one of the dominate reactions during synergetic pyrolysis. Among other volatile organic compounds, the system produced organic molecules with shorter C-chain (1–2 C atoms) at Stage 1, and then, benzene and larger molecules (4–6 C atoms) were generated mainly at Stage 2. This should be explained by the continuous chain scission and free radical reactions after ester scission. In the residual chain of PET, the carbons at the ends (and adjacent atoms) were more likely to escape, due to the reaction with free radicals, thus generating smaller molecules with 1–2 C atoms. Afterwards, the benzene ring, which was originally located at the middle of the chain, was exposed to the end and thus reacted, generating larger molecules with 4–6 C atoms. In addition, the formation of alkenes and alkynes was possibly resulted from reduction reactions caused by free radicals. Therefore, the decarboxylation and free radical reaction played an essential role in NCM-PET pyrolysis as well. The produced free radicals and reducing gases (e.g., CO and CO_2) not only contributed to the pyrolysis of PET, but also played key roles in the decomposition and reduction of NCM.

Reaction mechanisms

The DFT calculation was applied to optimize the models and investigate the binding energies between PET and NCM molecules. The polar (001) surface was reported with low surface energy and large surface area, according to previous studies, and thus was chosen as the slab model surface[32,33]. The variables of different adsorption configurations can be described as follows. The Li, TM, and O served as terminations of NCM (001) slab, while the vertical and horizontal planes of the benzene ring were possible adsorption postures of PET. The O, C, and H were adsorption sites on PET. After optimization, the binding energies of each adsorption configuration were summarized in Table 1, while a lower adsorption energy represented an easier generation of a more stable configuration. The exact configurations for each model were demonstrated in Supplementary Figs. S2–S5.

For the PET adsorption on the Li surface, more Li-O bonds were formed with lower adsorption energies, when the PET was in horizontal position. Configurations 1, 2, and 3 were similar in both configuration type and adsorption energy after optimization (Supplementary Fig. S2 of SI), implying that the O atoms in ester and carboxyl groups were likely to form single bonds with 1-3 Li atoms on the surface of NCM (001) slab. As the plane of four O was parallel to Li surface, due to lying benzene, the 6-8 Li-O bonds were generated for each PET model and the lowest adsorption energy was −4.248 eV. The O (Configuration 4) and H (Configuration 5) in vertical PET were found combinative to Li surface as well, but the combination was much weaker because of the higher adsorption energy. The PET adsorption on the TM surface also showed preference in horizontal position, but with a weaker combination (adsorption energy as −2.760 eV) than that on the Li surface. For horizontal PET (Configuration 6), 2 O and 2 C atoms in the PET were adsorbable to the TM surface, forming 4O/C-TM bonds. Vertical PET allowed only single O-TM or H-TM bond in each configuration (Configurations 7–10) with very weak combination especially regarding H-TM combination. The interaction between PET and O surface was negligible with the adsorption energy closing to 0. In general, PET showed an evident bonding preference on Li over TM and O. Moreover, horizontal PET tended to be adsorbed more easily, compared with the vertical one. This should be attributed to the simultaneous multiple bonding allowed by the planar distribution of atoms on and around the benzene rings. In addition, the O served as the most active atom in PET and provided stronger bonds to NCM (Li and TM), in comparison with the C and H atoms.

Taking all the findings into consideration, the synergetic effect between PET and NCM could be comprehensively discussed. The synergetic effect basically refers to the phenomenon that the existence of PET and NCM alters the pyrolysis behaviors of each other, which is because of the reaction between the two reactants and their pyrolysis intermediate products as well. The changes in pyrolysis behaviors were evident by comparing our experimental results to pure reactants as discussed before. On one side, the decomposition of NCM was evidently accelerated as a result of PET in the reaction system, that is, the starting temperature of the thermal decomposition was dropped to 400 °C and the effective Li-TM separation was completely finished at only 550 °C. On the other side, the degradation of PET was prolonged to stages of higher temperatures when NCM was co-pyrolyzed. The reasons for the synergetic effect could be explained as below. First, the early decomposition of NCM was accelerated by the surface adsorption between PET and NCM as shown in Fig. 5. Pure NCM possessed high thermal stability and remained non-reactive even at 800 °C. With the addition of PET in the reaction system, the O atoms in the PET were adsorbable to metal atoms in the NCM, and the capture on Li was stronger than that on TM. The preference for Li can be explained by the weak ionic

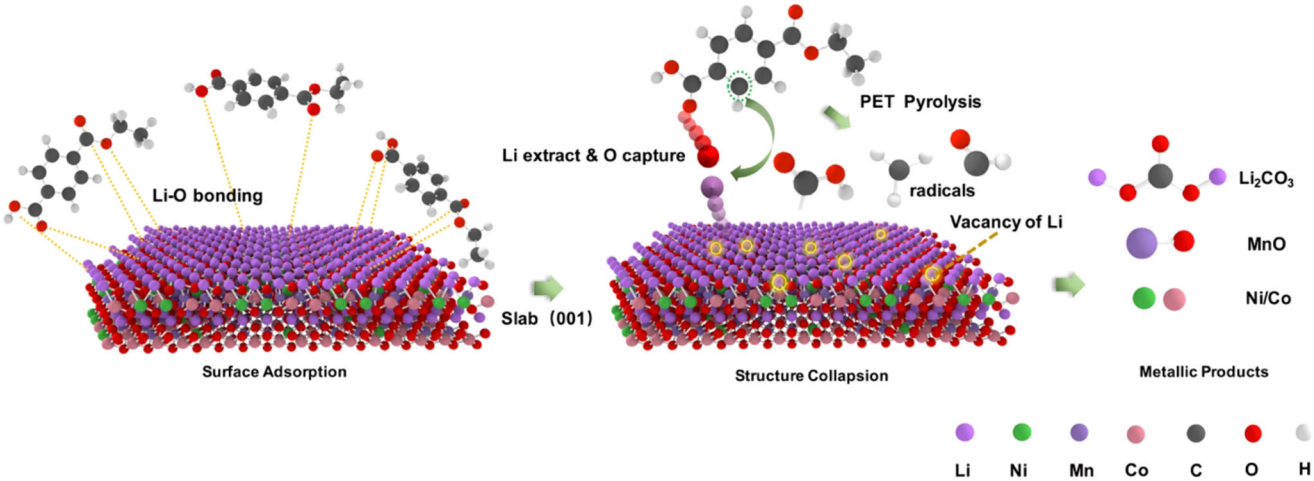

Fig. 5 | Schematic diagram created by the authors by using VESTA illustrating the synergetic pyrolysis mechanisms of PET + NCM ($LiNi_{1/3}Co_{1/3}Mn_{1/3}O_2$), where PET is polyethylene terephthalate.

bonds between Li atoms and NCM lattice, which were much more fragile and easily broken compared with the covalent bonds of the TM. As a result, the Li-O adsorption bonding extracted Li from the NCM and led to the production of Li_2CO_3 and earlier formation of Li vacancy in NCM lattice. As a support, the synergetic pyrolysis of NCM and other O-containing plastics was conducted (Supplementary Fig. S7). After pyrolyzed with polybutylene terephthalate (PBT) and polymethyl methacrylate (PMMA), the NCM was decomposed to Li_2CO_3, TM oxides, and alloys as well. Meanwhile, the partially collapsed lattice structure with Li vacancy was unstable, and thus the remained TM and O in the octahedron framework of the NCM formed metal oxides. As a support of Li escape and lattice collapse, the XRD patterns in Fig. la confirmed the formation of Li_2CO_3, MnO, and $Ni_xCo_{1-x}O$ at 550 °C and the formation of $Ni_xCo_{1-x}O$ at higher temperatures. Second, the products of PET pyrolysis accelerated NCM reduction. The pyrolysis of PET released various free radicals and reductive gaseous products, including carboxylic acid, CO, CO_2, CH_4, etc. Previous studies revealed that the reducing gases were more attractive to the O atoms in NCM and caused the continuous O escaping and bond breaking in NCM[18,34]. The indispensable role of the PET on the stepwise reduction of TM was well proved by the transformation from $Ni_xCo_{1-x}O$ to $Ni_xCo_{1-x}O$ with the PET increasing from 1.0:0.2 to 1.0:0.3 (Fig. 1c). Moreover, the synergetic effect and changes in thermal behaviors of NCM and PET were in agreement with the coupling reaction mechanisms as proposed previous studies[18,24]. This phenomenon implied that a low-temperature reaction (PET pyrolysis) could reduce the energy barrier of a high-temperature one (NCM decomposition). In addition, the reason of prolonged PET degradation could be explained by the consumption of free radicals caused by NCM, which slowed down the self-catalysis reaction of PET degradation.

Metal recovery and NCM regeneration

Figure 6a shows the recycling process for NCM recycling with synergetic pyrolysis of PET plastics. After synergetic pyrolysis, water washing was adopted for effective separation of Li from TM, because the soluble Li_2CO_3 can be easily extracted from the solid phase (Sample SP). By means of a simple filtration process, the Li_2CO_3 could be concentrated in the leachate and was crystalized after drying (Sample P-Li). Meanwhile, the insoluble particles in the solid phase (Sample P-TM) were mainly composed of metal oxides, elemental transition metals and PET-derived carbon. As expected, the typical XRD patterns in Fig. 6b verified a successful Li-TM separation. It is obvious that Li_2CO_3 was formed in the Sample P-Li with simultaneous formation of MnO and Ni_xCo_{1-x} in Sample P-TM. The XRD results also suggested that water washing could successfully separate Li_2CO_3 from the TM phases, based on the difference in solubility. The recovery ratio of each element was further illustrated in Fig. 6c, which implied that more than 99% of Li was recovered in Sample P-Li and over 99% of Ni, Co, and Mn could be recycled in Sample P-TM. The recovery ratio of Li showed slightly higher than 100%, which was caused by the experimental errors caused by operation, detection, and the variation of the samples. Besides, Ni, Co, and Mn were not detectable in Sample P-Li and no Li was found in Sample P-TM, thus revealing that water washing could achieve high efficiency and selectivity for the separation of Li and TM. The as-obtained Sample P-Li and P-TM, possessing high metal purity, could be potentially used as feedstocks for practical applications.

In this work, Sample P-Li and P-TM, viewed as potential battery raw materials, were employed to regenerate NCM cathode materials, and the XRD patterns in Fig. S1 supported the crystal structure of regenerated NCM. By solid-state sintering, the following equations (Eqs. 1 and 2) were expected to take place, inducing the crystallization of new NCM from Li and TM precursors and the calcination of organic compounds with the participation of oxygen. Thus, the sintering step regenerated NCM and removed residual carbon simultaneously.

$$6\,Li_2CO_3 + 4\,Ni + 4\,Co + 4\,MnO + 7O_2 \rightarrow 12\,LiNi_{1/3}Co_{1/3}Mn_{1/3}O_2 + 6\,CO_2 \quad (1)$$

$$4\,C_xH_yO_z + (4x + y - 2z)O_2 \rightarrow 4x\,CO_2 + 2y\,H_2O \quad (2)$$

As evidenced in Fig. 6b, the XRD pattern of the regenerated NCM showed that NCM crystal phase of high purity was observed with sharp peaks, which are corresponding to the α-$NaFeO_2$ structure. This confirmed that the regenerated NCM could be well crystallized with the above solid-state sintering method. Meanwhile, no peaks of other crystal phases were observed, suggesting a complete participation of Li/TM feedstocks and phase transformation to NCM. The doublet peaks of (008)/(110) and (006)/(102) split clearly and sharply, which was considered as crucial indicator for the layer structure in NCM cathode materials[35,36]. The morphology and microstructure of the regenerated NCM materials were further characterized by SEM and HR-TEM. Figure 6d showed the micro-scale spherical particle was agglomerated by regular nano-scale polyhydron particles with a typical size of 200–800 nm. The morphology was similar to previous studies on NCM cathode materials, which revealed the restoration of the crystal structure[37–39]. Previous studies also reported that small particle size and uniform distribution were beneficial for the cycling and C-rate performances of NCM, and certain agglomeration could enhance electrochemical charge-discharge performance, owing to better ionic conductivity provided by the inter-connection between particles[40]. HR-TEM image in Fig. 6e showed two sets of clear fringes, and the inter-planar spacing was observed

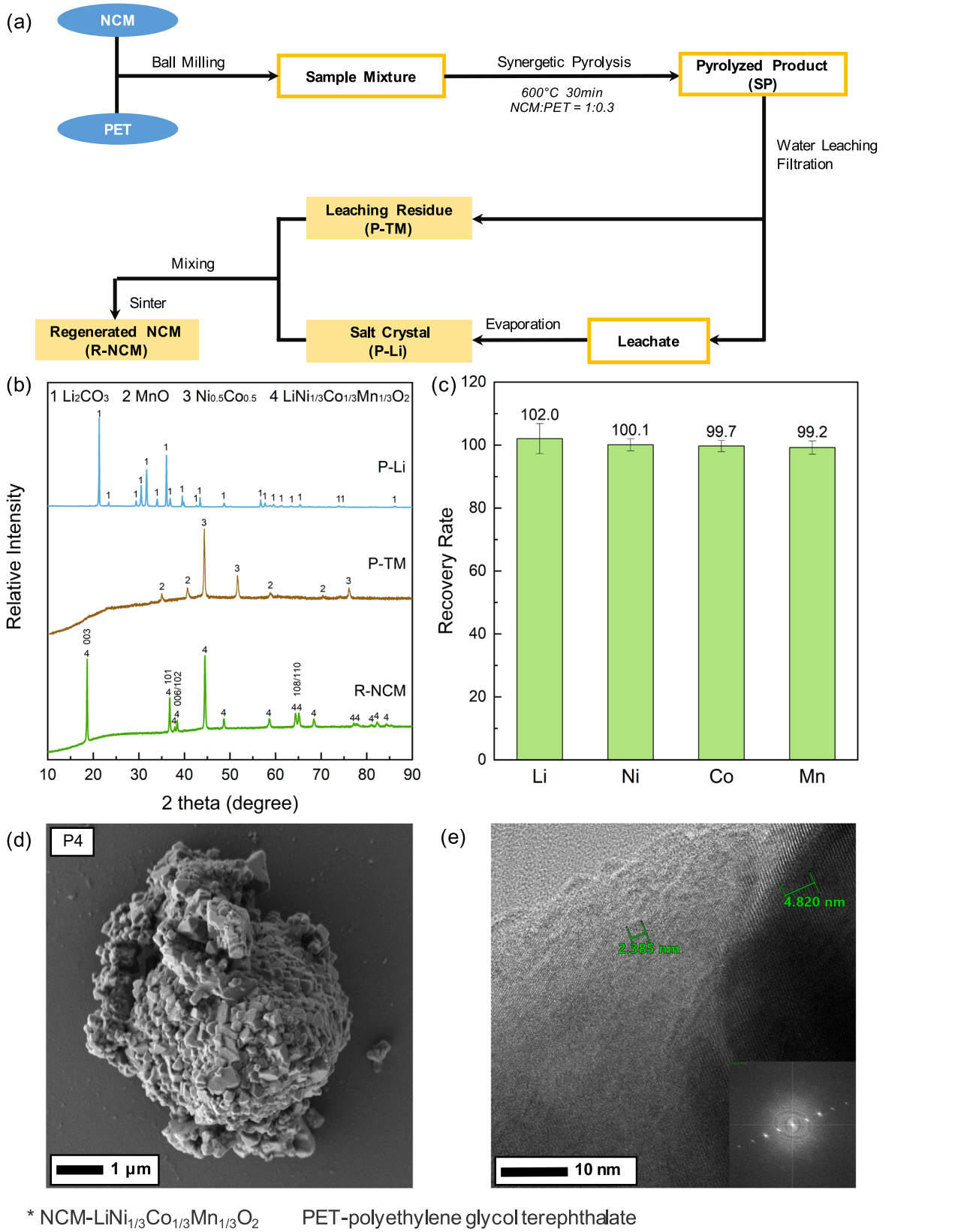

Fig. 6 | Whole recycling process and characteristics of recycling products. a A schematic diagram showing the recycling process of the NCM powder with synergetic pyrolysis of PET plastics, where NCM is $LiNi_{1/3}Co_{1/3}Mn_{1/3}O_2$, PET is polyethylene terephthalate, R-NCM is regenerated NCM, P-TM is transition metal products, and P-Li is Li products; (**b**) XRD patterns of the post-treatment products, including Sample P-Li, P-TM, and R-NCM; (**c**) content of Li, Ni, Co, and Mn in Sample P-Li and P-TM, and each content was provided with an error bar which was calculated via standard deviation of three parallel tests; (**d**) typical SEM and (**e**) typical HR-TEM images of Sample R-NCM, including the inset showing the corresponding fast Fourier transform (FFT) image.

as 0.48 nm and 0.24 nm, assigned to the (003) and (101) planes of NCM, respectively. The FFT (fast Fourier transform) pattern revealed that the particle was preferentially exposed with (003) plane, which was consistent with the above XRD results, thus verifying a typical (003) crystal plane of the layered phase in the regenerated NCM cathode materials. In addition, the electrochemical performance of the regenerated NCM cathode materials was tested by making coin cell batteries (Supplementary Fig. S8). The discharge capacity reached over 151 mAh/g and 121 mAh/g current density of 0.1 C and 1 C, respectively, and the retention rate was 85.4% after 40 cycles.

Discussion

Until most recently, many studies have focused on recycling spent cathode materials via pyrolysis strategy, and some of them need to reply on additional chemicals to overcome critical technical challenges, such as high energy consumption, low lithium recovery ratio and secondary pollution, etc. The carbon-contained reductants were chosen as one of the environmentally friendly reducing agents for pyrolysis process. However, high reaction temperatures are still required for achieving high recovery ratio of metal elements. To achieve economic feasibility, it is highly desirable to develop energy saving process for pyrolysis recycling of battery materials. It is well known that PET is one of the most widely used polymers for disposable plastic products, which contributed to a tremendous volume of waste generation, thus leading to serious environmental concerns. PET can be decomposed into fuel sources by catalytic reactions, with simultaneous generation of large amounts of free radicals and gases, which could greatly reduce the pyrolysis temperature for the thermal decomposition of the other co-pyrolyzation substances. Inspired by this phenomenon, this study proposed a facile synergetic pyrolysis strategy for NCM-PET system, which was highly efficient for element recovery and beneficial to both economy and environment.

The results of this study suggested that the synergetic pyrolysis system could greatly reduce the decomposition temperature of NCM to 550 °C with the simultaneous generation of Li_2CO_3, $Ni_xCo_{1-x}O$, Ni_xCo_{1-x}, and MnO as the product phases. Meanwhile, the PET addition of 1.0:0.3 (NCM/PET mass ratio) was enough to complete the decomposition reaction within only 30 min. The results in this work were further compared with previous studies, as shown in Supplementary Table S2. For instance, when coke, graphite or carbon were used as reductants, the pyrolysis temperatures were typically in the range of 650–1000 °C, with a duration time of 60–180 min. Meanwhile, the complete decomposition of NCM was achieved with only 550 °C within 30 min, much lower than previous work. In addition, owing to relatively low pyrolysis temperature, high retention of the valuable metal elements (over 99%) in the pyrolyzed products was confirmed, especially for the volatile Li element. This energy saving strategy was potentially applicable for efficient recovery of valuable metals (e.g., Li, Ni, Co, and Mn) from spent LIBs through simple post treatment (e.g., water washing). It should be emphasized that disposal and resource utilization of the plastic waste was demonstrated for battery recycling technology, taking the production of NCM and PET in 2023 as an example, over 12% of PET would be utilized according to this strategy. Thereafter, a simple but efficient water-washing step could successfully separate Li and TM with high recovery ratio (over 99%) and high purity (no impurity metals detected). In addition, new NCM material with well layered structure was successfully regenerated by sintering the recovered Li- and TM-precursors at 800 °C, and the residual carbon was simultaneously decomposed under air atmosphere. It should be mentioned that more detailed physicochemical properties and electrochemical performances of the regenerated NCM materials will be reported in future work. Furthermore, this study proposed the synergetic pyrolysis effect between the two particles and explained their interaction influences on each other. The exploration of reaction mechanisms provided theoretical basis for industrial applications and migration applications. Overall, this study provided thinking of using plastic properties to achieve a win-win situation by simultaneous treatment of plastic waste and battery wastes for valuable metal recovery.

Conclusion

This study proposed an NCM recovery strategy by NCM-PET synergetic pyrolysis which is highly efficient and beneficial to both economy and environment. Meanwhile, the reaction mechanisms were intensively explicated for insight understanding and guidance of further application. The NCM was prefixed with PET powder with a mass ratio of 1.0:0.3, and then the mixture was synergetically pyrolyzed under 550 °C within 30 min, and NCM was transformed to more uniform phases including Li_2CO_3, MnO, $Ni_xCo_{1-x}O$, and Ni_xCo_{1-x}. A simple following leaching step successfully separated Li and transition metals, and the Li, Ni, Co, and Mn were all recovered with high purity and recovery ratio (over 99%). The whole treatment process was environmentally friendly and required no other chemicals. In addition, new NCM material with well layered structure was also regenerated using the recovered Li and TM. The comprehensive analysis of experimental data and theoretical calculation revealed two core mechanisms of the synergetic pyrolysis. First, the O on horizontal PET favored bonding with Li on NCM (001) surface, leading to the Li extraction of Li in NCM and accelerated the lattice failure. Second, the degradation of PET released active free radicals and reductive gases, which caused O capture and stepwise reduction of transition metals. Consequently, the proposed NCM-PET synergetic pyrolysis served as an idea solution as it utilized PET plastics and was chemical-free; reduced both reaction temperature and duration; achieved high recovery efficiency and purity, and pointed out the synergetic effect between NCM and PET, which provided theoretical basis for the application in industry and migration applications.

Methods

Materials and reagents

Battery grade $LiNi_{1/3}Co_{1/3}Mn_{1/3}O_2$ (NCM333) powder sample received from Shenzhen Kejing Zhida Technology Co., Ltd. was used in this work, instead of spent cathode materials. PET sample was received from Qingdao Usolf Chemical Technology Co., Ltd. The molecular weight of PET was about 20520, and the polydispersity was 1.43. Polybutylene terephthalate (PBT) and polymethyl methacrylate (PMMA) samples were received from Hubei Chaode Chemical Technology Co., Ltd. Note that no other chemicals or reagents were employed in the pyrolysis and post-treatment processes. For metal element quantification, HCl (37 wt%), HNO_3, and H_2O_2 (30 wt %) (volume ratio 9:3:1) of analytical grade were purchased from Shanghai Aladdin Bio-Chem Technology Co., Ltd., and used as the digestion solution.

Synergetic pyrolysis and sample characterization

The effects of three key factors, including temperature, NCM:PET mass ratio, and dwelling time on crystal phase change were systematically investigated in this study. The dried NCM and PET powder were mixed via ball-milling (QM-QX-2L, MITR) at 3000 rpm for 30 min. The effect of PET addition on crystal phase change was studied using six gradients of NCM:PET mass ratio (1.0:0.1, 1.0:0.2, 1.0:0.3, 1.0:0.4, 1.0:0.5, and 1.0:1.0). The sample mixture was then added into a quartz crucible and placed in a tube furnace (OTF-1200X-II-100, Kejing., China) for synergetic pyrolysis. The pyrolysis was conducted under N_2 atmosphere with a flow rate of 0.3 L min^{-1}, and a heating rate of 10 °C min^{-1}. To individually explore the effect of pyrolysis temperature, the mixture was heated at different target temperatures (400, 500, 550, 600, 700, 800, 900, and 1000 °C) for a fixed time (120 min), and the effect of dwelling time on crystal phase change was investigated by heating at a fixed temperature (400 °C) for different dwelling time (15, 30, 60, 90, and 120 min). The effect of other O-containing polymers was observed by applying PBT and PMMA plastics. The plastic and NCM was mixed with an NCM/plastic mass ratio of 1.0:0.5, and the mixture was then pyrolyzed at 550 °C for 60 min.

X-ray diffraction (XRD, Rigaku SmartLab) technique was applied to identify the phase transformation behavior during the pyrolysis, and the XRD patterns were recorded under monochromated Cu $K_{\alpha 1}$ radiation operating at 45 kV and 200 mA from 10 to 90° (10° min^{-1}). To determine the content of metals in the pyrolyzed products, the solid products were digested with acids and metal elements (Li, Co, Ni, and Mn) were quantified

by inductively coupled plasma-optical emission spectrometry (ICP-OES; 8000 PerkinElmer). The morphology and element distribution of the products were obtained by the scanning transmission electron microscopy-energy dispersive X-ray (STEM-EDX) by a Tecnai G2 F30 (Thermo Fisher) microscope operating at an accelerating voltage of 300 kV. The mass change of all pyrolysis samples was recorded to calculate the loss of ignition (LOI).

In particular, the thermal behavior of the blended NCM/PET system, especially regarding evolutionary components, was monitored using a thermogravimetric analysis (TGA, 209F1, NETZSCH) coupled with mass spectroscopy (MS, QMS403C, NETZSCH) and a Fourier transform infrared spectroscopy (FT-IR, Nicolette-IS-50, Thermo Fisher) separately. Typically, 30 mg of the NCM-PET mixture with a mass ratio of 1.0:1.0 was loaded in an alumina crucible, and the thermal behavior was monitored from 30 to 1000 °C under N_2 atmosphere with a heating rate of 10 °C min^{-1}.

Post-treatment and sample characterization

The products obtained under the optimal pyrolysis condition (marked as Sample SP) were washed with the deionized water at room temperature to separate Li and TM elements. Sample SP was added into the deionized water with a solid/liquid ratio of 20 g/L, and then the mixture was treated with a shaker (TS-212N, TENSUC) at 100 rpm for 60 min[16,41,42]. After simple washing, the solid residue (denoted as Sample P-TM) was filtered and separated from the leachate. The leachate was then evaporated under 90 °C to obtain another solid product (Sample P-Li). The supposed Li- and TM-concentrated products were denoted as Sample P-Li and P-TM, respectively.

The content of all metal elements in the post-treatment products was quantified by ICP-OES after acid digestion, to determine the purity of the product and the metal recovery ratio of the progress. The recovery ratio of the targeted metal elements in the recovered products was calculated with the below Eq. (3):

$$R_i = \frac{m_P \cdot wt\%_{iP}}{m_R \cdot wt\%_{iR}} \times 100\% \quad (3)$$

where $wt\%_{iP}$ and $wt\%_{iR}$ are the weight content of metal "*i*" in the recovered product (P, referring to Sample P-Li or P-TM) and the raw NCM-PET mixture (*R*), respectively; m_P and m_R are the weight of recovered product and raw mixture, respectively. All samples were tested three times and the error bars were calculated by standard deviation.

The weight content was calculated as Eq. (4):

$$wt\%_i = \frac{c_i \cdot V}{m} \times 100\% \quad (4)$$

where c_i, *V*, and *m* are the concentration of metal *i* in the digested solution, the volume of the digested solution and the mass of the digested sample, respectively.

The new NCM was then resynthesized by using the recovered Sample P-Li and P-TM in previous steps. After confirming the content of Li in Sample P-Li and the content of Ni, Co, and Mn in Sample P-TM, the two solid samples were weighed to reach the molar ratio of Li:TM (Ni + Co + Mn) = 1.1:1.0 and then fully mixed by ball-milling at 3000 rpm for 30 min. The as-obtained solid mixture was then transferred to a muffle furnace (KSL-1200X-M, Kejing., China) and sintered at 800 °C for 10 h with a ramping rate of 5 °C min^{-1} under air atmosphere, resulting in the regenerated NCM (Sample R-NCM). XRD was applied to identify the crystal phases in the solid products. Scanning electron microscope (SEM) was performed to observe the sample morphology on a FEI Nova NanoSem 450. High-resolution TEM (HR-TEM) data were collected to characterize the microscopy in nano-scales. The electrochemical performance of the regenerated materials was carried out by using CR 2032 type coin cell at 30 °C. The cathode materials were prepared by mixing with active materials (70 wt%), PVDF (15 wt%), and acetylene black (15 wt%). The as-prepared electrodes were dried at 120 °C for 12 h, and then assembled with lithium anode and $LiPF_6$ solution electrolyte in the Ar-filled glovebox (Mikrouna, Germany). Charge-discharge tests were measured on LAND Battery Test System (Wuhan, China) with the voltage between 2.7 and 4.3 V at the current density of 1 C. Rate performance was carried out at the current density of 0.1 C, 0.2 C, 0.5 C, 1 C, 2 C, and 0.1 C.

DFT calculation

DFT calculation was carried out to harvest the adsorption preference of NCM and PET particles. Spin-polarized DFT calculations were performed using the Vienna ab initio simulation package (VASP)[43,44]. The generalized gradient approximation proposed by Perdew, Burke, and Ernzerhof (GGA-PBE) was selected for the exchange-correlation potential[45]. The pseudo-potential was described by the projector-augmented-wave (PAW) method[46]. The geometry optimization was performed until the Hellmann–Feynman force on each atom was smaller than 0.02 eV/Å. The energy criterion was set to 10^{-6} eV in iterative solution of the Kohn-Sham equation. The single PET monomer was constructed as simplified PET to make calculation feasible. The NCM (001) slab model was constructed by cleaving the (001) surface of LCO unit cell and expanding into a 4a*5b*c supercell, and the Co atoms were randomly replaced by 1/3 Ni and 1/3 Mn atoms. Li, TM, or O terminations on the slab model surface were investigated and compared. 18 Å vacuum above the slab model was created. During optimization, only the top three layers of atoms were allowed to relax. The adsorption energy (E_{ads}) was calculated according to Eq. (5)

$$E_{ads} = E_{total} - E_1 - E_2 \quad (5)$$

in which E_{total} is the DFT energy of NCM (001) with PET adsorbed, E_1 is NCM (001) energy and E_2 is PET energy.

Data availability

The data that support the findings of this study are available from the corresponding author upon reasonable request.

Code availability

The code that supports the findings of this study is available from the corresponding author upon reasonable request.

Received: 24 November 2023; Accepted: 31 October 2024;
Published online: 23 November 2024

References

1. Makuza, B., Tian, Q., Guo, X., Chattopadhyay, K. & Yu, D. Pyrometallurgical options for recycling spent lithium-ion batteries: A comprehensive review. *J. Power Sourc.* **491**, 229622 (2021).
2. Miao, Y., Liu, L., Zhang, Y., Tan, Q. & Li, J. An overview of global power lithium-ion batteries and associated critical metal recycling. *J. Hazard. Mater.* **425**, 127900 (2022).
3. Makuza, B., Yu, D., Huang, Z., Tian, Q. & Guo, X. Dry Grinding-Carbonated ultrasound-assisted water leaching of varbothermally reduced lithium-ion battery black mass towards enhanced selective extraction of lithium and recovery of high-value metals. *Resourc. Conserv. Recycl.* **174,** 105784 (2021).
4. Yu, Z., Lu, F., Zou, Y. & Yang, X. Quantifying energy flexibility of commuter plug-in electric vehicles within a residence–office coupling virtual microgrid. Part II: Case study setup for scenario and sensitivity analysis. *Energy Build.* **254,** 111552 (2022).
5. Harper, G. et al. Recycling lithium-ion batteries from electric vehicles. *Nature* **575**, 75–86 (2019).
6. Global Industry Analysts, Inc. *Lithium-ion (Li-ion) batteries-global strategic business report*. https://www.researchandmarkets.com/reports/4805605/li-ion-battery-global-market-trajectory-and#rela3–5021667 (access date: Dec 2022).

7. Xiao, J., Guo, J., Zhan, L. & Xu, Z. A cleaner approach to the discharge process of spent lithium ion batteries in different solutions. *J. Clean. Prod.* **255,** 120064 (2020).
8. Velázquez, M., Valio, Santasalo, A., Reuter & Serna, G. A critical review of lithium-ion battery recycling processes from a circular economy perspective. *Batteries* **5,** 68 (2019).
9. Chen, Y. et al. Thermal treatment and ammoniacal leaching for the recovery of valuable metals from spent lithium-ion batteries. *Waste Manag.* **75**, 469–476 (2018).
10. Ren, J. et al. The impact of aluminum impurity on the regenerated lithium nickel cobalt manganese oxide cathode materials from spent LIBs. *N. J. Chem.* **41**, 10959–10965 (2017).
11. Fan, E. et al. Low-temperature molten-salt-assisted recovery of valuable metals from spent lithium-ion batteries. *ACS Sustain. Chem. Eng.* **7**, 16144–16150 (2019).
12. Peng, C., Liu, F., Wang, Z., Wilson, B. P. & Lundström, M. Selective extraction of lithium (Li) and preparation of battery grade lithium carbonate (Li_2CO_3) from spent Li-ion batteries in nitrate system. *J. Power Sources* **415**, 179–188 (2019).
13. Lin, J. et al. Environmentally benign process for selective recovery of valuable metals from spent lithium-ion batteries by using conventional sulfation roasting. *Green. Chem.* **21**, 5904–5913 (2019).
14. Lin, J. et al. Conversion mechanisms of selective extraction of lithium from spent lithium-ion batteries by sulfation roasting. *ACS Appl. Mater. Interfaces* **12**, 18482–18489 (2020).
15. Di, C. et al. in *Energy Technology 2020: Recycling, Carbon Dioxide Management, and Other Technologies The Minerals Metals & Materials Series* Ch. 37, 387–395 (Springer International Publishing, 2020).
16. Tang, Y. et al. Recovery and regeneration of $LiCoO_2$-based spent lithium-ion batteries by a carbothermic reduction vacuum pyrolysis approach: controlling the recovery of CoO or Co. *Waste Manag.* **97**, 140–148 (2019).
17. Liu, C., Lin, J., Cao, H., Zhang, Y. & Sun, Z. Recycling of spent lithium-ion batteries in view of lithium recovery: a critical review. *J. Clean. Prod.* **228**, 801–813 (2019).
18. Zhao, Y. et al. Regeneration and reutilization of cathode materials from spent lithium-ion batteries. *Chem. Eng. J.* **383,** 123089 (2020).
19. Zhang, B. et al. A sodium salt-assisted roasting approach followed by leaching for recovering spent $LiFePO_4$ batteries. *J. Hazard. Mater.* **424**, 127586 (2022).
20. Zhou, F. et al. Vacuum pyrolysis of pine sawdust to recover spent lithium-ion batteries: the synergistic effect of carbothermic reduction and pyrolysis gas reduction. *ACS Sustain. Chem. Eng.* **10**, 1287–1297 (2022).
21. Lan Tiseo. Market volume of polyethylene terephthalate worldwide from 2015 to 2021, with a forecast for 2022 to 2029. https://www.statista.com/statistics/1245264/polyethylene-terephthalate-market-volume-worldwide/.
22. Çit, İ. et al. Comparative pyrolysis of polyolefins (PP and LDPE) and PET. *Polym. Bull.* **64**, 817–834 (2009).
23. Dimitrov, N., Kratofil Krehula, L., Ptiček Siročić, A. & Hrnjak-Murgić, Z. Analysis of recycled PET bottles products by pyrolysis-gas chromatography. *Polym. Degrad. Stab.* **98**, 972–979 (2013).
24. Singh, R. K., Ruj, B., Sadhukhan, A. K. & Gupta, P. A TG-FTIR investigation on the co-pyrolysis of the waste HDPE, PP, PS, and PET under high heating conditions. *J. Energy Inst.* **93**, 1020–1035 (2020).
25. Xu, J. et al. Compatibilization of isotactic polypropylene (iPP) and high-density polyethylene (HDPE) with iPP–PE multiblock copolymers. *Macromolecules* **51**, 8585–8596 (2018).
26. Chakraborty, A., Kunnikuruvan, S., Dixit, M. & Major, D. T. Review of computational studies of NCM cathode materials for Li-ion batteries. *Isr. J. Chem.* **60**, 850–862 (2020).
27. Kramer, D. & Ceder, G. Tailoring the morphology of $LiCoO_2$: a first principles study. *Chem. Mater.* **21**, 3799–3809 (2009).
28. Guo, Y. et al. Efficient degradation of industrial pollutants with sulfur (IV) mediated by $LiCoO_2$ cathode powders of spent lithium-ion batteries: a "treating waste with waste" strategy. *J. Hazard. Mater.* **399**, 123090 (2020).
29. Özsin, G. & Pütün, A. E. TGA/MS/FT-IR study for kinetic evaluation and evolved gas analysis of a biomass/PVC co-pyrolysis process. *Energy Convers. Manag.* **182**, 143–153 (2019).
30. Honus, S., Kumagai, S., Fedorko, G., Molnár, V. & Yoshioka, T. Pyrolysis gases produced from individual and mixed PE, PP, PS, PVC, and PET—part I: production and physical properties. *Fuel* **221**, 346–360 (2018).
31. Honus, S., Kumagai, S., Molnár, V., Fedorko, G. & Yoshioka, T. Pyrolysis gases produced from individual and mixed PE, PP, PS, PVC, and PET—part II: fuel characteristics. *Fuel* **221**, 361–373 (2018).
32. Hong, L. et al. Electronic structure of $LiCoO_2$ surfaces and effect of Al substitution. *J. Phys. Chem. C* **123**, 8851–8858 (2019).
33. Bennett, J. W., Jones, D., Huang, X., Hamers, R. J. & Mason, S. E. Dissolution of complex metal cxides from first-principles and thermodynamics: cation removal from the (001) surface of $Li(Ni_{1/3}Mn_{1/3}Co_{1/3})O_2$. *Environ. Sci. Technol.* **52**, 5792–5802 (2018).
34. Xiao, J., Li, J. & Xu, Z. Novel approach for in situ recovery of lithium carbonate from spent lithium-ion batteries using vacuum metallurgy. *Environ. Sci. Technol.* **51**, 11960–11966 (2017).
35. Xi, Y. et al. Comparative study of the electrochemical performance of $LiNi_{0.5}Co_{0.2}Mn_{0.3}O_2$ and $LiNi_{0.8}Co_{0.1}Mn_{0.1}O_2$ cathode materials for lithium ion batteries. *Solid State Ion.* **327**, 27–31 (2018).
36. Jiang, T. et al. Improved high-potential property of Ni-tich $LiNi_{0.8}Co_{0.1}Mn_{0.1}O_2$ with a garnet ceramic LLZTO surface modification in Li-ion batteries. *ACS Appl. Energy Mater.* **5**, 305–315 (2021).
37. Li, J., Yao, R. & Cao, C. $LiNi_{1/3}Co_{1/3}Mn_{1/3}O_2$ nanoplates with 010 active planes exposing prepared in polyol medium as a high-performance cathode for Li-ion battery. *ACS Appl. Mater. Interfaces* **6**, 5075–5082 (2014).
38. Meng, X. et al. Recycling of $LiNi_{1/3}Co_{1/3}Mn_{1/3}O_2$ cathode materials from spent lithium-ion batteries using mechanochemical activation and solid-state sintering. *Waste Manag.* **84**, 54–63 (2019).
39. Dang, H. et al. Lithium leaching via calcium chloride roasting from simulated pyrometallurgical slag of spent lithium-ion battery. *Sep. Purif. Technol.* **233**, 116025 (2020).
40. Huang, D. et al. Nanoscale $LiNi_{0.5}Co_{0.2}Mn_{0.3}O_2$ cathode materials for lithium-ion batteries via a polymer-assisted chemical solution method. *Appl. Mater. Today* **16**, 342–350 (2019).
41. Hu, J., Zhang, J., Li, H., Chen, Y. & Wang, C. A promising approach for the recovery of high value-added metals from spent lithium-ion batteries. *J. Power Sourc.* **351**, 192–199 (2017).
42. Hekmatfar, M., Kazzazi, A., Eshetu, G. G., Hasa, I. & Passerini, S. Understanding the electrode/electrolyte interface layer on the Li-rich nickel manganese cobalt layered oxide cathode by XPS. *ACS Appl. Mater. Interfaces* **11**, 43166–43179 (2019).
43. Kresse, G. Efficiency of ab-initio total energy calculations for metals and semiconductors using a plane-wave basis set. *Comput. Mater. Sci.* **6**, 15–50 (1996).
44. Kresse, G. & Furthmüller, J. Efficient iterative schemes for ab initio total-energy calculations using a plane-wave basis set. *Phys. Rev. B* **54**, 11169 (1996).
45. Perdew, J. P., Burke, K. & Ernzerhof, M. Generalized gradient approximation made simple. *Phys. Rev. Lett.* **77**, 3865 (1996).
46. Blöchl, P. E. Projected augmented-wave method. *Phys. Rev. B* **50**, 17953 (1996).

Acknowledgements

The authors are grateful to the National Natural Science Foundation of China (42277403; 41977329), and the Natural Science Foundation of Guangdong Province (2021B1515020041), Guangdong Provincial Key Laboratory of Soil

and Groundwater Pollution Control (No. 2023B1212060002), and High-level University Special Fund (G03050K001) for financial support. Also, we want to thank the Center for Computational Science and Engineering at Southern University of Science and Technology (SUSTech), and core research facilities at SUSTech to provide quality resources and services. X.-Y.L. would like to thank the financial support from Hong Kong Environment and Conservation Fund (No.: 39/2019) and Hong Kong Competitive Research Funding Schemes for the Local Self-financing Degree Sector Faculty Development Scheme (No.: UGC/FDS25/E06/19).

Author contributions

All the people who have made substantial contributions to the work are reported in the manuscript. The authors' major contributions and affiliation are listed below: Zhe Meng: Conceptualization, Methodology, Validation, Investigation, Data curation, Formal analysis, Writing-Original draft preparation, Writing-Reviewing and Editing. Jinchuan Dai: Conceptualization, Methodology, Validation, Investigation, Data curation, Formal analysis, Writing- Original draft preparation, Writing-Reviewing and Editing. Xiao-Ying Lu: Conceptualization, Methodology, Writing- Reviewing and Editing. Kehua Wu: Methodology, Writing- Reviewing and Editing. Yonghong Deng and Jun Wang: Resources, Methodology, Writing-Reviewing and Editing. Kaimin Shih: Resources, Supervision, Writing-Reviewing and Editing. Yuanyuan Tang: Conceptualization, Methodology, Resources, Supervision, Project administration, Funding acquisition, Writing-Reviewing and Editing.

Competing Interests

The authors declare no competing interests.

Additional information

Supplementary information The online version contains supplementary material available at https://doi.org/10.1038/s44172-024-00317-x.

Correspondence and requests for materials should be addressed to Yuanyuan Tang.

Peer review information *Communications Engineering* thanks Muhammad Imran Yaqub and the other, anonymous, reviewers for their contribution to the peer review of this work. Primary Handling Editors: [Grace Wan-Ting Chen] and [Mengying Su and Saleem Denholme].